Tissue Shape Acquisition with a Hybrid Structured Light and Photometric Stereo Endoscopic System

Marco Visentini-Scarzanella[1], Tatsuya Hanayama[1], Ryunosuke Masutani[2], Shigeto Yoshida[3], Yoko Kominami[3], Yoji Sanomura[3], Shinji Tanaka[3], Ryo Furukawa[2], Hiroshi Kawasaki[1]

[1] Department of Information Systems and Biomedical Engineering, Kagoshima University
[2] Department of Endoscopy and Medicine, Hiroshima University
[3] Department of Intelligent Systems, Hiroshima City University

Abstract. *In situ* 3D reconstruction from endoscopic images is important to determine the correct course of action for, e.g., treatment of abnormal growths. Currently, the endoscopist has to rely solely on visual cues in order to infer the growth's shape and size and determine an appropriate treatment. However, tissue uniformity and scale ambiguity from traditional monocular endoscopes make this visual assessment prone to errors and time consuming. We propose a practical system to densely reconstruct both shape and size of tissues with minimal modifications to a standard endoscope. We present a custom single-fiber structured light probe projecting a wave pattern on the tissue surface that allows semi-dense reconstruction with few ambiguities. Based on the coarse reconstruction, we retrieve the surface reflectance parameters according to a hybrid diffuse/specular model which are used to initialise a close-range Photometric Stereo reconstruction. By taking into account the tissue characteristics and the light fall-off, our Photometric Stereo formulation provides dense metric 3D shape information without the need for surface normal integration. A preliminary study was carried out both on phantoms and *ex vivo* samples of human tissue.

1 Introduction

In recent development of endoscopy technology, diagnosis and treatment using endoscopes on digestive tracts have been widely performed [1]. As for the treatment of early stage gastric cancers, treatment methods differ depending on the size of the tumours. For this reason, accurate measurement of the size of neoplasias is important. Currently, forceps and 2D visual cues are used by the endoscopist to assess the size of polyps, but this is error-prone and time consuming. Therefore, techniques for objective measurements are desirable.

Intraoperative 3D reconstruction from endoscopic images has been the focus of extensive research in recent years, and a comprehensive review of the state-of-the-art can be found in [2, 3]. However, as many of the systems mentioned in the review article such as stereo or Structure-from-Motion require either costly stereo cameras or multiple images, solution to the one-shot reconstruction problem remains elusive. Indeed, in the recent evaluation of one-shot 3D reconstruction technique [3], 6 out of 8 methods

require a stereo camera, whereas the remaining two are Structured Light and Time-of-Flight systems. Structured light (SL) is one of the systems that can solve the one-shot reconstruction problem that has seen recent applications in endoscopy: in [4], a micro pattern projector was mounted outside the endoscope for 3D reconstruction, in [5] a SL device for tubular structures was proposed, while sparse reconstruction with spectral encoding was studied in [6]. However, generally a sparse reconstruction of a limited area can be obtained, and noise as well as tissue texture can prevent large areas from being reconstructed and obtain reliable size information.

Earlier works in depth cue fusion [7] suggested combining sparse, reliable feature-based methods such as structured light with dense photometric-based techniques that can be initialised with sparse information. Photometric-based techniques such as Shape-from-Shading have been applied to endoscopy [8–10], but they require either pre-operative data for registration, prior calibration procedures, or intra-operative calibration to resolve the scaling ambiguity and recover absolute depth. Photometric Stereo (PS) is a technique that has been applied to endoscopy [11] on Lambertian surfaces, but required external markers for initialisation of the illumination response matrix. Recent developments in PS [12] allow direct computation of the depth without integration of the normal field after sparse depth initialisation.

In this work, we contribute by proposing a SL endoscope with an integrated projector in its instrument channel. We improve the PS formulation for endoscopes by using the sparse reconstruction to initialise a PS technique that is independent of the surface albedo and explicitly takes into account light intensity distribution and position, while being robust to non-Lambertian areas. Importantly, our system does not require significant alterations to standard equipment. To the best of our knowledge, this is the first work combining structured light and photometric stereo applied to endoscopy. Preliminary results on phantoms and *ex vivo* human tissue samples show interesting possibilities for further research.

2 Method

Our proposed system consists of two main modules: first, we miniaturised a laser pattern projector consisting of a single optical fiber that can be fed through the instrument channel of the endoscope for SL projection. Second, the PS module consists of three externally mounted LEDs. While our prototype does not satisfy the endoscope size requirements due to the external mount, in the final product stage it will be possible to include three internal LEDs, or to apply colour filters to the on-board lighting as done in [11]. The overall system with the projected lights and patterns is shown in Fig. 1a, 1b. Reconstruction with the SL module is discussed in Section 2.2, while the final PS-based reconstruction is presented in Section 2.3. Prior to the reconstruction, however, together with the standard camera and photometric calibration, it is necessary to calibrate the SL and LED setup. This is discussed in the next section.

2.1 LED and Structured Light calibration

Following camera and photometric calibration, calibration of extrinsic matrix relating the SL projector with the endoscope camera is performed following the steps outlined

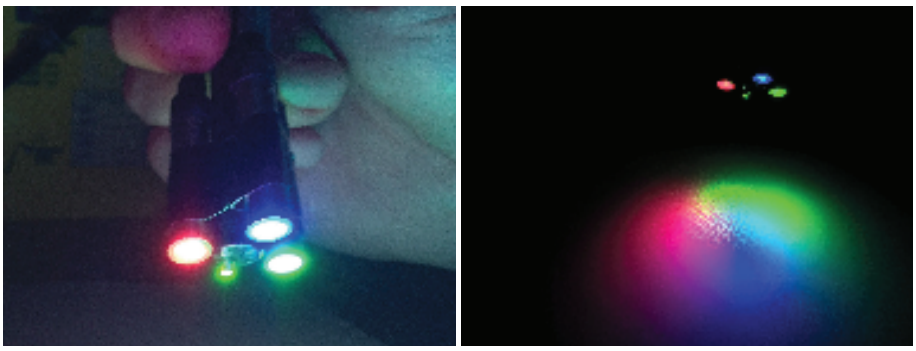

(a) (b)

Fig. 1: (a) Close-up of the prototype. The structured light projector protrudes from the tool channel, while the three red, green and blue LEDs are mounted around the scope. (b) Projected patterns from LEDs and structured light.

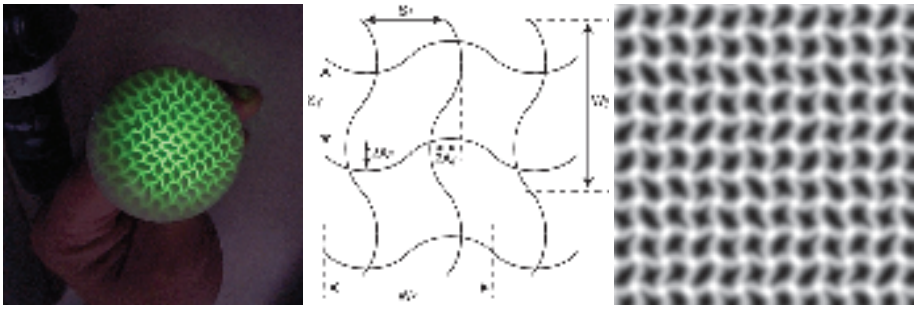

(a) (b) (c)

Fig. 2: (a) Calibration sphere with projected SL pattern. (b) Design of the wave pattern. (c) Projected SL pattern.

in [4]: images of a spherical object with known dimensions are taken while projecting the SL pattern as shown in Fig. 2a. A known pixel is used for initial matching between the projected and visualised patterns, while the distinctive crossing points of the wave pattern allow to find unique matches for calibration refinement. The wave pattern used is adapted from [13] and is shown in Fig. 2b. The wave lines are sinusoidal patterns, with equal wavelengths between vertical and horizontal lines. However, since the vertical spacing is not equal to an integer multiple of the horizontal wavelength, the intersection points (or grid points) appear at the different phases on the wave patterns (Fig. 2c). This implies that the local pattern around an intersection point has a local uniqueness, which can be used as a helpful discriminative feature both during calibration as well as reconstruction. While our current prototype assumes the SL projector to be fixed relative to the camera, this is seldom the case during endoscopy since the tool channel

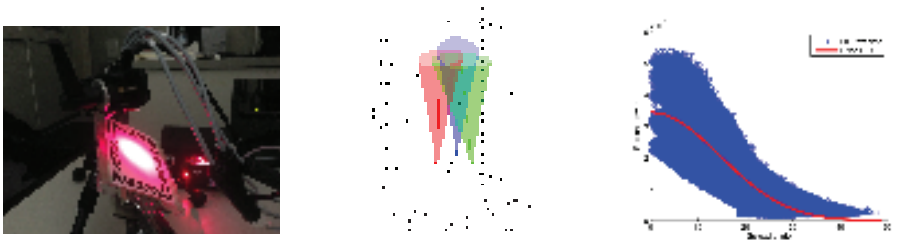

(a) (b) (c)

Fig. 3: (a) RID calibration for red LED. (b) Estimated position and orientation of LEDs. (c) Estimated RID.

might be needed for other purposes. We therefore proposed a system for auto-update of the calibration parameters, to appear in [14].

One of the crucial stage is accurate calibration of the LED setup. While this traditionally only involves positional calibration of the LEDs, which is achieved usually through triangulation of specular highlights, it is also necessary to estimate the Radiance Intensity Distribution (RID) of the light sources. The RID is a function $g(\phi)$ describing the power emitted by a light source according to the angle ϕ from its main axis. This is important since virtually all models used in SFS and PS assume an 'omnilight' model where the light emits radiance isotropically in all directions, and the incident light energy on the surface is only attenuated by the light fall-off inversely proportional to the square of the distance. However, as verified also in [11], this model is inadequate to the illumination types found on scopes, where the highly focused light is normally emitted up to 15°-30°from the main direction. To this end, we have recently proposed a system (to appear in [15]) for joint practical calibration of light position and RID. The technique leverages the fact that the projection of a light beam on a Lambertian plane will be symmetrical about an axis related to its position and orientation. Also, we prove that the point of maximum intensity lies on said axis, hence it is possible to recover the light position and orientation just by looking at its points of local maxima. In Fig. 3a, we show a frame from the red LED calibration, done with a matte calibration plane with AR markers for positional information around a blank space for RID calibration. The estimated position of the LEDs is shown in Fig. 3b, reflecting the triangle formation around the central camera (black point), while the fitted RID to the information is shown in Fig. 3c. While the absolute amplitude of the RID is only of relative importance since it depends on the material reflectance, the important aspect to calibrate is the RID fall-off, estimated in our experiment to get to 10% of its amplitude at approximately 25°. This corresponds to an analytical expression for the RID of $g(\phi) = \cos(\phi)^{15.58}$, which will be used in our PS reconstruction.

2.2 Structured light shape acquisition

Our structured light system configuration is shown in Fig. 4(a). This consists of a FujiFilm VP-4450HD system coupled with a EG-590WR scope. The pattern projector is

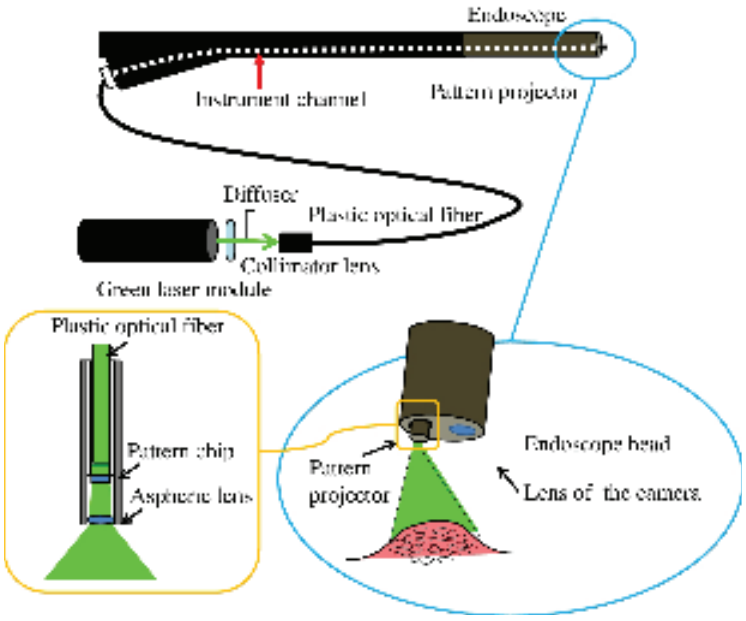

Fig. 4: (a) Proposed structured light endoscopic setup

inserted through the instrument channel of the scope, with the projector lens slightly protruding from the head. The light source of the projector is a green laser module with a wavelength of 532nm. The laser light is transmitted through a plastic optical fiber with a diameter of 1.8mm to the tip of the projector. A micro pattern chip with the printed pattern is set at the tip of the fiber. The transmitted light passes through the micro pattern chip and then through the aspherical lens, with a field of view of 30°.

For the structured light shape acquisition, our method is based on template matching using grid-point features in [16]. In this system, given a wave intersection template dictionary, matches are searched along epipolar lines. Since the matching process can be affected by the pattern distortion as it is projected on the surface, this distortion is represented as an affine transformation with two DOFs. Finally, the overall template matching cost is estimated using the optimal surface normal directions given the affine transformation matrix. The patch-based template matching cost is then regularized by Belief Propagation according to the cost function:

$$E(T) = \sum_{p \in V} D(p, t_p) + \sum_{(p,q) \in U} W(t_p, t_q), \tag{1}$$

where $T = \{t_p | p \in V\}$ is a set of correspondences with t_p, t_q being the corresponding grid point of pattern points p and q respectively, V is the set of the grid points, D is the correlation cost between the grid points of the image and the pattern, and W is a distance cost which is 0 if p and q are neighbouring grid points and positive otherwise.

This cost function is small if p and t_p have small matching cost D, and the connections between the grid points are coherent for the image and the pattern.

2.3 Photometric stereo reconstruction

Multispectral Photometric Stereo (MPS) [17] traditionally aims to recover surface normals from a single image of a Lambertian surface simultaneously illuminated by a red, blue and green light. In this way, the intensity recorded by each colour channel roughly corresponds to the reflected light from one of the light sources. More formally:

$$I = \rho(P \cdot L)\mathbf{n}, \tag{2}$$

where ρ is the monochromatic albedo, P is the matrix representing the spectral crosstalk between CCD sensors, L the concatenated light directions and $\mathbf{n}$ the target surface normals. Traditionally, methods involve a sparse reconstruction using Structure-from-Motion to estimate P, after which the normals can be found from a simple matrix inversion given the known light positions [17]. While PS in the general Computer Vision community can benefit from a number of simplifying assumptions such as a larger number of inputs and directional lighting, in MIS the problem is highly challenging. Only recently Collins and Bartoli [11] adapted the MPS problem to close-range lighting, recovering depth through a 2-stage local/global approach. However, they maintain the assumptions of uniform albedo, Lambertian reflectance through the use of polarising filters, and assume the presence of external tools/markers to estimate the unknown matrix P. More recently, in [12] a Fast Marching (FM) based procedure was proposed for close-range PS, which starting from a single known point, or 'seed', propagates the information while explicitly taking into account the light RID and distance attenuation.

We build on these past improvements by proposing a novel technique that considers a more realistic reflectance model with specularities. Moreover, we adapt the propagation method in [12], for explicit depth reconstruction independent of the albedo and integrated with our structured light initialisation. First, similarly to [17] with Structure-from-Motion and PS, we use our SL reconstruction to estimate the matrix P and calculate $\tilde{I} = P^{-1}I$, the crosstalk-compensated image. Then, we consider the Blinn-Phong model for diffuse/specular reflection:

$$\tilde{I} = \frac{g\,(\mathbf{v}\cdot\mathbf{a})}{\|\mathbf{l}\|^2}\left(\rho_1\frac{\mathbf{l}\cdot\mathbf{n}}{\|\mathbf{l}\|\|\mathbf{n}\|} + \rho_2\left(\frac{(\mathbf{l}+\mathbf{v})\cdot\mathbf{n}}{\|\mathbf{l}+\mathbf{v}\|\|\mathbf{n}\|}\right)^{\alpha}\right), \tag{3}$$

where $g()$ is the light RID estimated through calibration [15], $\mathbf{l}$ the light vector at a point, $\mathbf{v}$ the view vector, (ρ_1, ρ_2) the diffuse and specular albedos and α the exponent determining the sharpness of specularities. One of the nice characteristics of the Blinn-Phong model, apart from approximating well surfaces with specularities, is the additive relationship between diffuse and specular components, which we exploit in our method.

We notice that in Minimally Invasive Surgery (MIS) specularities are very sharp due to tissue characteristics and focused lighting. This implies a very high α, which in turn implies that the specular term will be essentially zero for $\frac{(\mathbf{l}+\mathbf{v})\cdot\mathbf{n}}{\|\mathbf{l}+\mathbf{v}\|\|\mathbf{n}\|} < 0.95$, meaning that most of the image will be essentially Lambertian apart from specularities that can be identified through intensity/saturation thresholding.

We therefore proceed first to reconstruct the diffuse portion of the surface. In [12] it is shown that the PS problem involving light sources with RIDs of the form $g(\phi) = \cos(\phi)^\beta$ amounts to solving the PDE:

$$\begin{cases} \mathbf{b}_{ij}(x,y,z) \cdot \nabla z(u,v) = s_{ij}(x,y,z), & (u,v) \in \Omega_p \\ z(u,v) = p(u,v), & (u,v) \in \partial\Omega_p \end{cases}, \tag{4}$$

where (x,y,z) are the 3D coordinates, (u,v) the pixel coordinates, $z(u,v)$ the function that maps a pixel value with its depth, $p(u,v)$ are Dirichlet boundary conditions and:

$$\mathbf{b}_{ij} = \begin{pmatrix} \tilde{I}_i(u,v) q_i^{\beta+3}(x,y,z) L_i^x - \tilde{I}_j(u,v) q_j^{\beta+3}(x,y,z) L_j^x \\ \tilde{I}_i(u,v) q_i^{\beta+3}(x,y,z) L_i^y - \tilde{I}_j(u,v) q_j^{\beta+3}(x,y,z) L_j^y \end{pmatrix}. \tag{5}$$

The vector $\mathbf{b}$ can be calculated from any pair of image channels (i,j) from the image intensity, the corresponding light source position (L^x, L^y), the distance q from the light source to a pixel and the RID parameter β. The scalar function $s(x,y,z)$ is:

$$s_{ij}(x,y,z) = \left(\tilde{I}_i(u,v) q_i^{\beta+3}(x,y,z) - \tilde{I}_j(u,v) q_j^{\beta+3}(x,y,z) \right) \frac{z(u,v)^2}{f}, \tag{6}$$

where f is the focal length. The solution to Eq. (4) can be found through the Fast Marching algorithm with the following forward upwind scheme, for the k^{th} iteration:

$$z^{k+1} = \frac{\|b_{ij}^1(z^k)\| z^k_{u-\mathrm{sgn}\left(b_{i,j}^1(z^k)\right),v} + \|b_{ij}^2(z^k)\| z^k_{u,v-\mathrm{sgn}\left(b_{i,j}^2(z^k)\right)} + s_{ij}(z^k)}{\|b_{ij}^1(z^k)\| + \|b_{ij}^2(z^k)\|}. \tag{7}$$

Finally, starting from our SL seeds, we can outline the Fast Marching algorithm:

1. Initialise SL seed values and add all the points' neighbours to a list of points to be visited. Initialise all other points to the depth of their nearest seed.
2. Traverse the list of points to be visited and calculate $\mathbf{b}$ and s for each point. Update the value of z according to a standard forward upwind scheme
3. Add the point's neighbours to the list of points to visit and repeat until convergence.

The algorithm above allows us to reconstruct Lambertian areas. However, it is adversely affected by specularities. In [12], the authors are able to 'steer' the propagation direction to propagate around cast shadows and avoid their interference in the propagation process. We propose the same strategy around specular highlights detected via standard intensity thresholding, so that the Lambertian portion of the image can be reconstructed error-free. Details on steering the Fast Marching propagation are in [12].

3 Results

We tested the performance of our proposed method on simulated data, phantom models and *ex vivo* human tissue samples. We first tested the PS and SL modules individually on simulations and phantom models respectively, while the full system was deployed

for the *ex vivo* tissue samples. All C++ code has been executed on a standard consumer grade laptop and is available on the author's site. In terms of computational complexity, a single iteration of the serial, unoptimised code for our algorithm was found to execute in 280ms for a 400×400 image on the CPU, with 3-4 iterations usually required until convergence. Given these timings, real-time operation is deemed to be feasible upon parallelisation of the fast marching algorithm.

3.1 Photometric Stereo evaluation

For our simulations, we used the *AbsPeaks* and *Sphere* datasets. The models were virtually placed at around 20mm and 60mm respectively, and were chosen to evaluate the performance of the algorithm on both smooth and irregular surfaces with discontinuities. The rendering was done by placing a virtual camera at the origin and three light sources with similar intrinsic characteristics as those founds on the endoscope used for our experiments. For each dataset, an artificial albedo with normalised values ranging from 0.6 to 1 was generated with a Perlin noise process in order to show the algorithm's independence to the object texture. This can be seen in the sample renderings in Fig. 5. The Blinn-Phong exponent for specularities was set to 100. To further evaluate the performance of our algorithm in noisy environments, we performed two tests: first, the input images were injected with i.i.d. noise drawn from a uniform distribution with ranges $[0, 0.05I_{max}]$ and $[0, 0.1I_{max}]$ respectively, where I_{max} is the maximum intensity of the image, corresponding to 5% and 10% noise respecitively. These results are shown in Table 1(a). Finally, we tested the sensitivity of the algorithm to errors in the initial seeds, by adding 5% and 10% noise to the initial seed values. Whenever a single input seed was used, this was placed in the middle of the image, and exactly 5% and 10% was added to its value. Whenever multiple seeds were used, the noise was drawn from a zero-mean uniform distribution and the seeds randomly placed across the dataset. These results are shown in Table 1(b). All results show a good performance of the algorithm under both noiseless and noisy conditions.

	Accuracy vs. Image noise		
	0%	*5%*	*10%*
Peaks */%*	0.04%	0.19%	0.38%
Peaks */mm*	0.01mm	0.04mm	0.08mm
Sphere */%*	0.08%	0.08%	0.23%
Sphere */mm*	0.05mm	0.05mm	0.14mm

(a)

	Accuracy vs. Seed noise		
	0%	*5%*	*10%*
Peaks - *Single seed*	0.04%	5.77%	11.65%
Peaks - *Multiple seeds*	0.04%	0.03%	0.02%
Sphere - *Single seed*	0.08%	5.618%	10.38%
Sphere - *Multiple seeds*	0.08%	0.12%	0.11%

(b)

Table 1: Reconstruction accuracy with absolute and relative errors for synthetic datasets against **(a)** image noise and **(b)** seed noise.

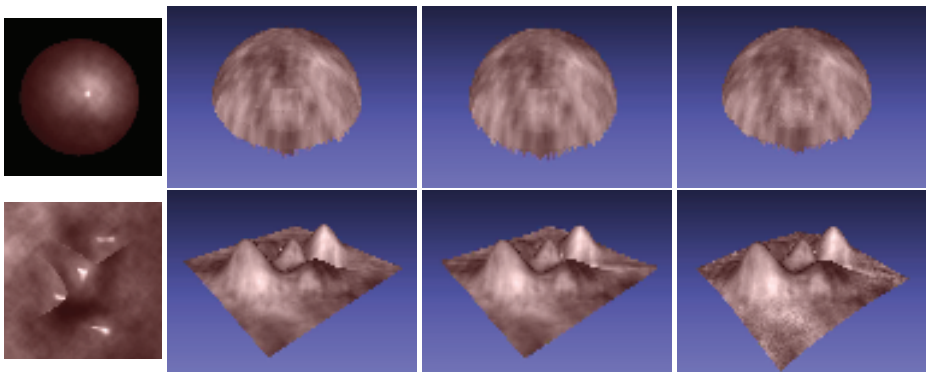

(a) (b) (c) (d)

Fig. 5: Reconstruction results for the Sphere (first row) and Peaks (second row) datasets. Columns (a-d) show an example rendered image from the dataset, the ground truth depth, and reconstruction results with no noise and 10% noise added respectively.

3.2 Structured Light evaluation

To evaluate the performance of our SL system, we test it first on an anatomical stomach model (Kyoto Kagaku) and then on a custom tumour phantom created to reproduce the reflectance characteristics of live tissue (Wetlab). The models were placed at approximately 7cm from the scope, reconstructed and their depth value at the point perpendicular to the scope compared with our manual measurements. Phantoms and renderings of their reconstructions are shown in Fig. 6. The SL reconstruction is able to successfully reconstruct the general trend of the surfaces, like the convexity of the phantom stomach in models (a) and (b), and the distance was measured to be within 5mm of its actual value. However, due to the lack of subpixel accuracy and the discreteness of disparity values, the reconstructions lack detail and exhibit some staircasing. In the tumour phantom for example, while there is a rise in the reconstructed volume corresponding to the lump, we are unable to clearly capture its boundaries. This aspect will be investigated as part of our future work, since a good initial reconstruction is crucial for correctly estimating the reflectance parameters needed by the PS module.

3.3 *Ex vivo* samples

In our experiments, *ex vivo* human tissue samples were collected and scanned at Hiroshima Hospital for qualitative validation. Three samples in total were collected during endoscopic resections of esophageal, gastric and colonic tumours. The samples were then fixed on a rigid support and scanned with our system. The input images to the system under multispectral and structured lighting are shown in Fig. 7 (top). The reconstruction renderings (bottom) are shown both with their true texture, while the inset images shown from the camera perspective are colour-coded to denote the reconstruction source: the red points represesent the initial structured light reconstruction, and the blue surface the final recovered shape.

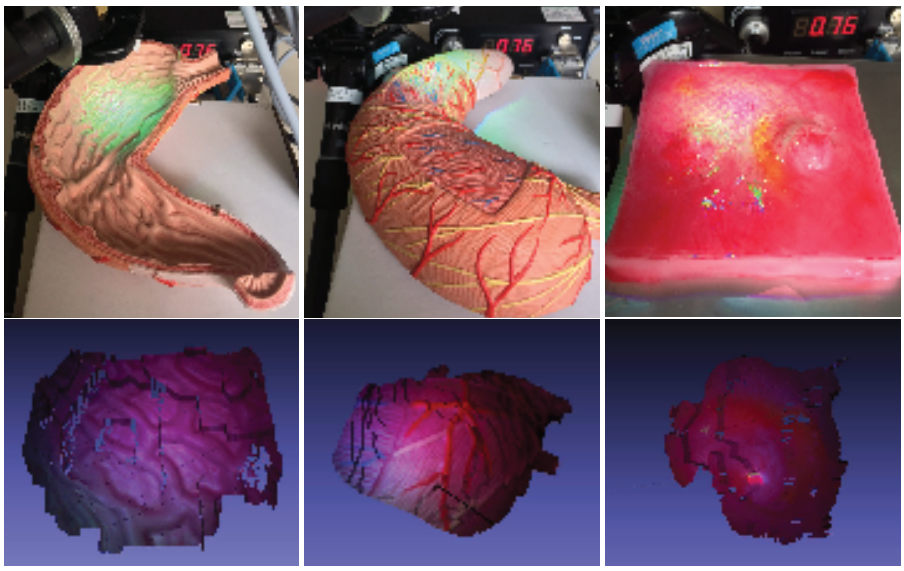

(a) (b) (c)

Fig. 6: SL evaluation. **Top:** images of (a),(b) anatomical stomach model and (c) tumour phantom. **Bottom:** their corresponding reconstruction renderings

In the first sample (Fig. 7(a)) the structured light pattern was clearly visible and a large central portion of the sample was reconstructed with structured light. The final propagated surface as seen from the camera perspective exhibits a largely flat trend, with a gentle downward slope towards the upper right, which is confirmed by visual assessment of the camera images. The oscillations on the side of the surface are due to the fact that in our current formulation each point exclusively considers information propagated along the shortest path, which means that it is affected by three seed points at most. Hence, any noise in neighbouring initial seeds will give rise to slight ripples in the surface. With our approach, it was possible to obtain the metric size of the complete sample rather than the smaller area that could be reconstructed with structured light.

In the second sample, the darker images only allowed to reconstruct a small portion of the surface. While the final propagated surface is piecewise flat, it clearly exhibits a protruding tip in correspondence of the white mass in the center of the sample. This was confirmed by additional images of the same sample, where while the high frequency details were lost, the overall trend of a flat surface with a central mass was successfully recovered. The flatness of the reconstruction is due mostly to the lack of subpixel accuracy in our SL initialisation, leading to a staircasing effect. We expect that for applications such as endoscopic navigation, with larger areas imaged, the method can benefit from a clearer contribution from the light fall-off and RID terms.

Finally, we show our third sample as a failure case, with the sample standing vertically on its base. The angle caused a noisy estimate of the seeds, leaving only a generic surface trend pointing towards the camera. Future work will aim to filter out noisy

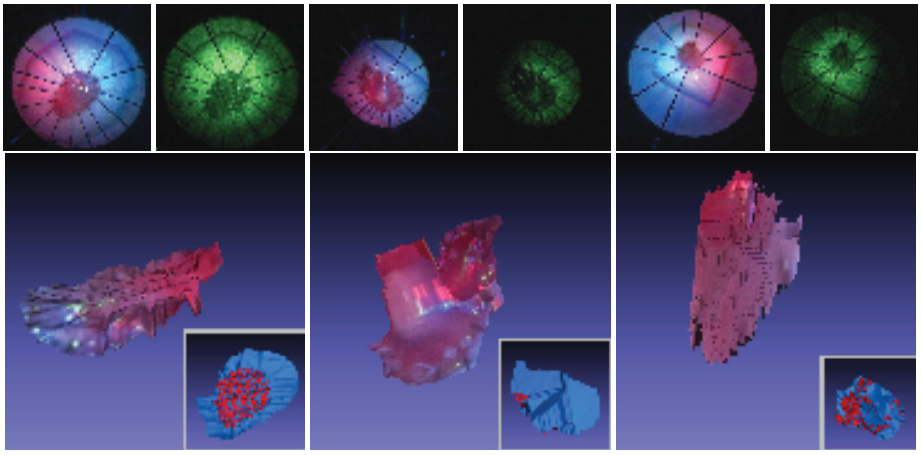

(a) (b) (c)

Fig. 7: *Ex vivo* samples. **Top:** SL and PS images of the collected samples. **Bottom**: reconstruction renderings with the real tissue texture. Inset, from the camera perspective, red points are the SL initialisation, the blue surface shows the final PS reconstruction.

seeds from the process. While imaging conditions as of now do not allow the recovery of smaller details, but can still be used for to assess the extent of the area.

4 Conclusions

We propose a hybrid Structured Light / Multispectral Photometric Stereo system for tissue size and shape acquisition in endoscopy. Our SL probe is small enough to fit through a standard instrument port, and the wave pattern employed allows reconstruction of a sharp monochromatic laser pattern with few ambiguities. We have adapted a state-of-the-art Fast Marching PS technique to the challenging MIS environment and showed its performance under noisy and textured environments with specularities. Promising preliminary results have been shown on simulated data and *ex vivo* human tissue samples showing a good ability to recover the overall size and general surface trend even in challenging conditions. Future work will focus on detailed reconstruction and integrating the LEDs inside the scope head in order to allow *in vivo* operation.

Acknowledgments

This work was supported by The Japanese Foundation for the Promotion of Science, Grant-in-Aid for JSPS Fellows no.26.04041.

References

1. Chadebecq, F., Tilmant, C., Bartoli, A.: How big is this neoplasia? live colonoscopic size measurement using the infocus-breakpoint. Medical Image Analysis **19**(1) (2015) 58 – 74

2. Maier-Hein, L., Mountney, P., Bartoli, A., Elhawary, H., Elson, D., Groch, A., Kolb, A., Rodrigues, M., Sorger, J., Speidel, S., Stoyanov, D.: Optical techniques for 3d surface reconstruction in computer-assisted laparoscopic surgery. Medical Image Analysis **17**(8) (2013) 974 – 996
3. Maier-Hein, L., Groch, A., Bartoli, A., Bodenstedt, S., Boissonnat, G., Chang, P.L., Clancy, N., Elson, D., Haase, S., Heim, E., Hornegger, J., Jannin, P., Kenngott, H., Kilgus, T., Muller-Stich, B., Oladokun, D., Rohl, S., dos Santos, T., Schlemmer, H.P., Seitel, A., Speidel, S., Wagner, M., Stoyanov, D.: Comparative validation of single-shot optical techniques for laparoscopic 3-d surface reconstruction. IEEE Transactions on Medical Imaging **33** (2014) 1913–1930
4. Furukawa, R., Aoyama, M., Hiura, S., Aoki, H., Kominami, Y., Sanomura, Y., Yoshida, S., Tanaka, S., Sagawa, R., Kawasaki, H.: Calibration of a 3d endoscopic system based on active stereo method for shape measurement of biological tissues and specimen. In: IEEE International Engineering in Medicine and Biology Conference (EMBC). (2014) 4991–4994
5. Schmalz, C., Forster, F., Schick, A., Angelopoulou, E.: An endoscopic 3d scanner based on structured light. Medical Image Analysis **16**(5) (2012) 1063 – 1072
6. Clancy, N.T., Stoyanov, D., Maier-Hein, L., Groch, A., Yang, G.Z., Elson, D.: Spectrally encoded fiber-based structured lighting probe for intraoperative 3d imaging. Biomedical Optics Express **2**(11) (2011) 3119–3128
7. Visentini-Scarzanella, M., Mylonas, G.P., Stoyanov, D., Yang, G.Z.: *i*-brush: A gaze-contingent virtual paintbrush for dense 3d reconstruction in robotic assisted surgery. In: Medical Image Computing and Computer-Assisted Intervention (MICCAI). (2009)
8. Wu, C., Narasimhan, S., Jaramaz, B.: A multi-image shape-from-shading framework fornear-lighting perspective endoscopes. International Journal of Computer Vision **86** (2010) 211–228
9. Malti, A., Bartoli, A.: Estimating the cook-torrance brdf parameters in-vivo from laparoscopic images. In: Workshop on Augmented Environment in Medical Image Computing and Computer Assisted Intervention (MICCAI), Nice, France (2012)
10. Ciuti, G., Visentini-Scarzanella, M., Dore, A., Menciassi, A., Dario, P., Yang, G.Z.: Intra-operative monocular 3d reconstruction for image-guided navigation in active locomotion capsule endoscopy. In: IEEE RAS EMBS International Conference on Biomedical Robotics and Biomechatronics (BioRob). (2012) 768 –774
11. Collins, T., Bartoli, A.: 3d reconstruction in laparoscopy with close-range photometric stereo. In: Medical Image Computing and Computer-Assisted Intervention (MICCAI). (2012)
12. Mecca, R., Wetzler, A., Bruckstein, A.M., Kimmel, R.: Near field photometric stereo with point light sources. SIAM Journal on Imaging Sciences **7**(4) (2014) 2732–2770
13. Sagawa, R., Sakashita, K., Kasuya, N., Kawasaki, H., Furukawa, R., Yagi, Y.: Grid-based active stereo with single-colored wave pattern for dense one-shot 3d scan. In: 3D Imaging, Modeling, Processing, Visualization and Transmission (3DIMPVT), 2012 Second International Conference on. (Oct 2012) 363–370
14. Furukawa, R., Masutani, R., Miyazaki, D., Baba, M., Hiura, S., Visentini-Scarzanella, M., Morinaga, H., Kawasaki, H., Sagawa, R.: 2-dof auto-calibration for a 3d endoscope system based on active stereo. In: IEEE International Engineering in Medicine and Biology Conference (EMBC). (2015)
15. Visentini-Scarzanella, M., Kawasaki, H.: Simultaneous camera, light position and radiant intensity distribution calibration. In: Pacific Rim Symposium on Image and Video Technology (PSIVT). (2015)
16. Kawasaki, H., Masuyama, H., Sagawa, R., Furukawa, R.: Single colour one-shot scan using modified penrose tiling pattern. IET Computer Vision **7**(5) (2013) 293–301
17. Vogiatzis, G., Hernandez, C.: Self-calibrated, multi-spectral photometric stereo for 3d face capture. International Journal of Computer Vision **97**(1) (2012) 91–103